INORGANIC CHEMISTRY

FRONTIERS

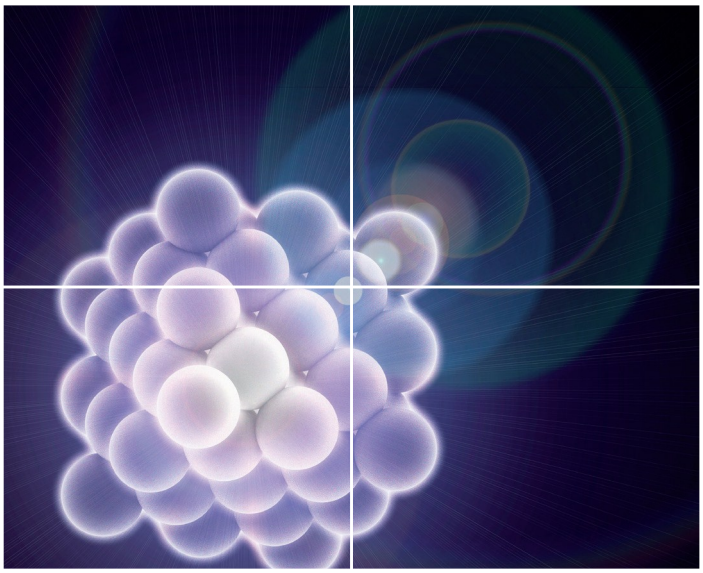

Accepted Manuscript

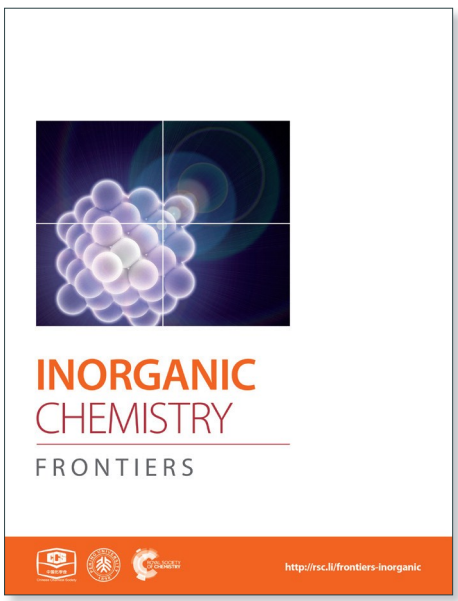

This is an *Accepted Manuscript*, which has been through the Royal Society of Chemistry peer review process and has been accepted for publication.

Accepted Manuscripts are published online shortly after acceptance, before technical editing, formatting and proof reading. Using this free service, authors can make their results available to the community, in citable form, before we publish the edited article. We will replace this *Accepted Manuscript* with the edited and formatted *Advance Article* as soon as it is available.

You can find more information about *Accepted Manuscripts* in the **Information for Authors**.

Please note that technical editing may introduce minor changes to the text and/or graphics, which may alter content. The journal's standard **Terms & Conditions** and the **Ethical guidelines** still apply. In no event shall the Royal Society of Chemistry be held responsible for any errors or omissions in this *Accepted Manuscript* or any consequences arising from the use of any information it contains.

Cite this: DOI: 10.1039/c0xx00000x

www.rsc.org/xxxxxx

ARTICLE TYPE

Novel, Fast-Processed Crystalline and Amorphous Manganese Oxide Nanoparticles for Stem Cell Labeling

Jessica M. Rosenholm,*[a,h,j] Riikka M. Korpi,[b,c] Eveliina Lammentausta,[b] Siri Lehtonen,[e] Petri Lehenkari,[d] Rasmus Niemi,[f,g] Wangchuan Xiao,[h] Jixi Zhang,[h,i] Desiré Lindberg,[j] Hongchen Gu,[h] Cecilia Sahlgren[f,g,k§] and Roberto Blanco Sequeiros*[b,l§]

Received (in XXX, XXX) Xth XXXXXXXXX 20XX, Accepted Xth XXXXXXXXX 20XX
DOI: 10.1039/b000000x

Magnetic resonance (MR) imaging, with its inherent good spatial resolution and without tissue penetration depth limitations associated to other cell tracking techniques, is considered a valuable tool to assess effects of cellular therapy. However, in order to allow *in vivo* tracking of transplanted cells with MRI, the cells must be labeled with contrast agents, usually in the form of magnetic or paramagnetic nanoparticles. Typically these are iron oxides, which are associated with a number of drawbacks related e.g. to generation of hypointensities to the MR image due to signal loss. In this study, two chemically distinct manganese oxide-based nanostructures were developed and their feasibility as labels for human mesenchymal stem cells (hMSCs) was investigated. The ability to monitor the produced particles alone or within labeled cells *in vitro* using MR imaging was further evaluated. Two novel synthetic approaches, the polyol process and microwave digestion, were combined to yield a "green", extremely rapid means of producing water-dispersible crystalline (MnO) and amorphous (MnOx) manganese oxides. To increase their water dispersability, capping agents in the form of organic polymers, poly(vinyl pyrrolidone) (PVP) and poly(acrylic acid) (PAA), were added in the synthesis process. Crystalline MnO was not formed when PAA was used as capping agent, since Mn ions (Mn^{2+}) cannot be hydrolyzed to $Mn(OH)_2$, which is an intermediate step in the formation of MnO, under the acidic conditions provided by PAA. PVP, on the other hand, served to induce a spherical shape to the formed nanocrystals. Remarkably, the relaxation times of the as-prepared amorphous MnOx were significantly shorter than those of their crystalline counterparts, and the biocompatibility was also higher for MnOx. To the best of our knowledge, this is the first report to describe the use of an amorphous MnOx as a cell label for MR imaging.

Introduction

Exogenous or autologous cell transplantation is regarded as a potential therapeutic method for a large variety of diseases. In the transplantation process, the ability to target and monitor transplanted cells is of critical importance. Magnetic resonance (MR) imaging offers non-invasive *in vivo* monitoring of cells labeled with suitable contrast agents with a high spatial resolution, additional anatomical and pathological details, and no exposure to ionizing radiation. The contrast agents serve to enhance the contrast of cellular targets in MR images by decreasing the relaxation times *T*1 (signal increase on the MR image) and/or *T*2 (signal loss on the MR image) to improve the image quality, acquisition time as well as enable enlargements of detectable organs/targets. For cellular labeling purposes, magnetic nanoparticles are of particular interest [1-3].

To date, small/ultra-small superparamagnetic iron oxide nanoparticles (SPIO/USPIO) have been the most widely used as contrast agents for cellular MR imaging [3-5]. Traditionally, these are prepared via the conventional coprecipitation method, which is difficult to control in terms of size distribution, crystallinity, saturation magnetization values as well as particle aggregation and dispersability in aqueous solutions [6,7]. To overcome these drawbacks, new synthesis approaches have been developed, such as high-temperature decomposition of iron precursors in nonpolar solvents, which produces high-quality monodisperse iron oxide nanoparticles with a tightly controlled size distribution and high crystallinity [7,8,9]. These particles are inherently hydrophobic, and needs to be either coated by a hydrophilic layer via surface functionalization procedures and/or phase transferred into water before they are suitable for biomedical applications. The addition of appropriate capping agents, such as carboxylic acids, in the synthesis process - resulting in hydrophilic groups on the formed particles has been an important development [10, 11]. Another method for producing intrinsically hydrophilic metal or metal oxide nanostructures with controlled properties is the polyol process, i.e. the reduction of metal salts in polyalcohols [6-8, 10-17]. When combined with microwave digestion, which is a well-established route in organic synthesis [18], this synthesis strategy may provide a simple, rapid (within minutes), effective, low energy-consuming, environmentally friendly "green" synthesis method for producing inorganic nanostructures with controllable characteristics as well [8, 14, 18, 19].

Gadolinium-based complexes, such as gadopentate dimeglumine, and manganese (Mn) both accelerate longitudinal *T*1 relaxation increasing signal intensity on MR images as opposed to iron oxides. However widely used in drug administration applications [20], gadopentate dimeglumine is associated with nephrogenic systemic fibrosis [21, 22] and is therefore a less favorable agent for clinical aim applications. The molecular size of gadopentate dimeglumine is also an issue. Whereas free manganese ions (Mn^{2+}) are also toxic and thus mainly applicable for animal manganese-enhanced MR imaging studies [23], manganese oxide (MnO) in crystalline form has a tolerable cellular toxicity range and is considered a promising agent for longitudinal cell tracking, as it is easy to deliver and maintains good image quality [23-25]. However, it is still controversial how the labeling with MnO affect cell function and cell differentiation capacity [26] and thus, there are only few studies reporting the use of MnO as a contrast agent for cellular tracking *in vivo*. Still, the obvious advantage of Mn-based substances related to the positive *T*1 contrast, which generates a signal increase that is opposite to iron oxide particles, opens up a multitude of opportunities in anatomical and functional imaging that can be used to augment tissue imaging. The effect could be especially beneficial in detecting metabolic events and adverse or pathological anatomy in tissue that has naturally low signal in MRI [24]. Various profits thus justify developing manganese-based nanoparticles for future clinical applications within molecular and cellular imaging.

The purpose of this study was to produce and characterize two chemically distinct types of manganese oxide, crystalline and amorphous, using the combined advantages of the polyol process and the microwave technique. We demonstrate the production of novel, water-dispersible (hydrophilic), fast-processed manganese oxide nanoparticles and assess the feasibility of these nanoparticles for labeling of human mesenchymal stem cells as well as MR imaging.

Materials & Methods

Preparation of manganese oxide nanoparticles

The manganese oxide syntheses were performed in a microwave reactor with a controllable temperature/heating and time program of a focused microwave synthesis system (Discover SClass, CEM, USA). In a typical synthesis, 12 mmol of sodium acetate was dissolved into 30 ml ethylene glycol by careful heating, ultransonication and stirring. When dissolved, 4 mmol of $MnCl_2 \cdot 4H_2O$ was added to the mixture and dissolved accordingly. The synthesis mixture was either used as such, or capping agents poly (acrylic acid), PAA (MW 5 000) or poly (vinyl pyrrolidone), PVP (MW 10 000) at an amount of Mn^{2+}: PAA/PVP = 1:2 (i.e. 8 mmol capping agent). The different reaction mixtures were then digested in the microwave at different temperatures (200ºC, 220 ºC, and 240 ºC) for different reaction times (5-50 min). After the reaction, quick cooling to room temperature was realized by high pressure air flow. The formed particles were precipitated by addition of 15 ml ethyl acetate and 3 ml absoluted ethanol, and separated by centrifugation at 7000 rpm for 10 min. The final particles were harvested by subsequent washing three times in ethanol, and redispersed in ethanol until further use. For ICP measurements, 100 µl of such suspension was dissolved into concentrated HNO_3 and diluted to 5 ml with ddH_2O.

Characterization

Transmission electron microscopy (TEM, JEOL 2010, at the Instrument Centre of Shanghai Jiao Tong University) was used for observing the morphology of the obtained nanoparticles. Hydrodynamic size was measured on either high performance particle sizer (HPPS 5001, Malvern Instruments Ltd., Worcestershire, UK) or a Malvern ZetaSizer (Malvern ZetaSizer NanoZS, Malvern Instruments Ltd., Worcestershire, UK) of which the latter also was used for zeta potential measurements. X-ray diffraction (XRD) was recorded on a Rigaku D/max 2250 VB/PC with CuKα radiation (1.54056 Å) at 40 kV, 200 mA to confirm the nanocrystalline phase. Manganese concentrations were determined by inductively coupled plasma emission spectroscopy (ICP, ICA P6300, Thermo Fischer, USA) after dissolution into concentrated HNO_3 with subsequent dilution into ddH_2O.

Relaxivity measurements

The relaxivity properties of the pure particle suspensions were measured on an NMR spectrometer (Minispec, mq60, Bruker, Germany). The proton resonance frequency was 60 MHz to assess their feasibility for MR imaging. The Carr-Purcell-Meiboom-Gill (CPMG) spin echo sequence was used for *T*2 measurements and saturation recovery sequence was used for *T*1 measurements. Known concentrations of particles, as determined from ICP, was diluted into water and kept at 37ºC prior to measurements. The transverse and longitudinal relaxation times in water of the as-prepared nanoparticles were measured at different Mn concentrations until the same value was provided by three consecutive measurements recorded.

Cell Viability

Viability was determined by WST-1 assay: Human mesenchymal stem cells were transferred to 96-well plates (9000 cells/well) and allowed to attach and grow. After 24 h, the medium was removed and replaced with 100 µl medium containing different concentrations of particles (10, 20 and 40µg/ml). After incubation for 2h, the medium was removed and replaced with particle free medium. At various time points after particle treatments 10 µl of WST-1 (Roche Applied science) reagent was added to cells and further incubated for 90 min, after which the 96-well plate was analyzed at 430 nm wavelength in a Varioskan plate reader to determine cell viability. Cell media without particles was used as a control.

MR imaging

For MR imaging measurements, crystalline (prepared at 240ºC for 30 min without additives) and amorphous (prepared at 240ºC for 20 min with PAA as additive) manganese oxide suspensions were diluted into agar at concentrations of 0.1 – 1 mM in 0.1 mM increments, and for more accurate relaxivity characterization, at concentrations of 0.01 – 0.1 mM in 0.01 mM increments were prepared and imaged with an MR scanner. The same suspensions in water were also pre-evaluated on the minispec instrument.

For MR imaging measurement of particle treated MSC cells, 125 000 MSCs were incubated with 20 and 40 µg/ml particles for 2h. Subsequently, the medium was replaced and the cells were allowed to grow for 24h after which the cells were harvested and pelleted in a 3% agar in eppendorf tubes.

*T*1 and *T*2 relaxation times of all the samples were measured using a 3T clinical MR scanner (Siemens Magnetom Skyra,

Siemens Healthcare, Erlangen, Germany) and a 8-channel receive-only small animal coil (RAPID Biomedical GmbH, Rimpar, Germany). *T*1 relaxation time was measured using single slice inversion recovery fast spin echo sequence (TR 10 000 ms, TE 8.6 ms, ten TI's between 50 and 9500 ms, FOV 12cm, matrix 256x256 yielding in-plane resolution of 0.47 mm, slice thickness 3 mm, ETL 8, NEX 1). *T*2 relaxation time was measured using multi-slice multi echo spin echo sequence (TR 1680 ms, 12 TE's between 11.5 and 138 ms, ETL 5; FOV, matrix and slice thickness unchanged). Slices were positioned along the cross-section of the test tubes. Circular ROIs were manually segmented into each test tube, and relaxation times were calculated pixelwise with non-linear fitting and assuming monoexponential relaxation using in-house MATLAB application (The MathWorks Inc., Natick, MA, USA). Mean value and standard deviation were calculated for each ROI.

Results

Synthesis and characterization of manganese oxides

When no capping agents were used in the synthesis protocols, 30 min at 240ºC proved to be sufficient for obtaining of a pale green synthesis mixture, characteristic of the formation of the crystalline MnO phase [23] as illustrated in Figure 1a. After purification and redispersion into ethanol, the obtained stable suspension was black in color and further TEM analysis revealed the presence of nanocrystals (Figure 1b). Based on this observation, together with ICP analysis (yield) the reaction temperature was set to 240 ºC and different reaction times (10, 20, 30 min) were evaluated for the manganese oxide syntheses together with capping agents PAA and PVP (Table 1). Interestingly, the use of PVP resulted in similar black suspensions after ethanol purification, whereas for the PAA-addition resulted in white suspensions (Figure 1c). TEM analysis of such a suspension suggested an amorphous structure had formed (Figure 1d). The distinction in the two different reaction systems is as follows. MnO (crystalline) was formed by two steps. Firstly, $Mn(OH)_2$ was formed by the hydrolysis of Mn^{2+} in the presence of CH_3COONa as alkalinity provider. The second step included the dehydration of $Mn(OH)_2$ at high temperature:

1) $Ac^- + H_2O = HAc + OH^-$
2) $Mn^{2+} + OH^- = Mn(OH)_2$
3) $Mn(OH)_2 = MnO + H_2O$

Therefore, MnO was not formed when PAA was used as capping agent, since Mn^{2+} cannot be hydrolyzed to $Mn(OH)_2$ under the acidic conditions provided by PAA (a polyacid). Moreover, the reaction of Mn^{2+} to MnO indicates that there is no oxidation or reduction reaction taking place in this system.

To determine the behavior in solution of the formed materials, whereby electron microscopy only provides information in dried state, the water/buffer suspensions of the amorphous and crystalline manganese oxides were investigated. Their suspension behavior especially in aqueous solvent is crucial for successful applicability, as the utilization of the produced materials, such as cellular labeling, will naturally take place under aqueous

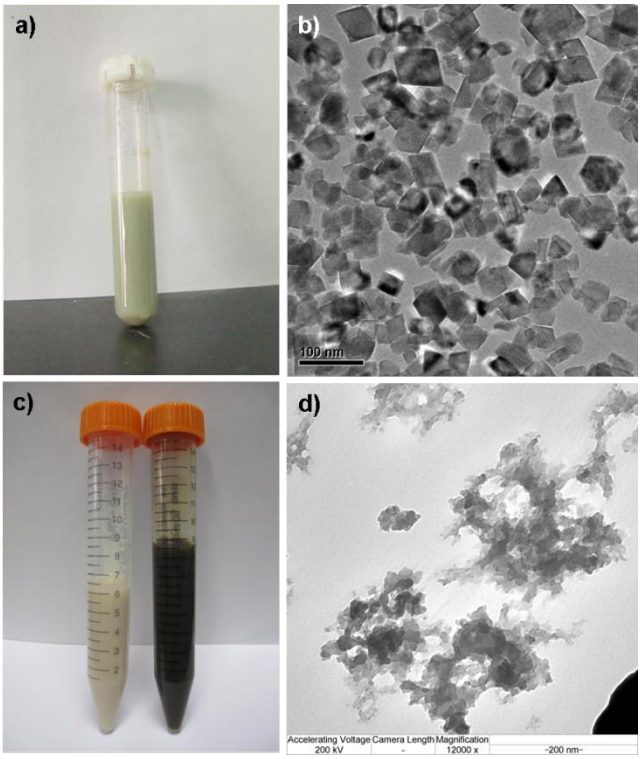

Fig.1 Image characterization of the formed manganese oxides. a) The synthesis mixture directly after microwave digestion when no additives were used; b) TEM image of a) after washing and dispersing into ethanol; c) ethanol suspensions of amorphous (white) and crystalline (black) manganese oxide; d) TEM image of the "white" suspension (using PAA as additive) indicating that an amorphous structure had formed.

conditions. Thus, their hydrodynamic size and net surface charge (zeta potential) at neutral pH were investigated with dynamic light scattering and electrokinetic measurements (Figure 2). For the crystalline sample, a hydrodynamic diameter of 99,17±0,17 nm (z-average) was found (Fig. 2a), with a low polydispersity index (PdI=0,076), indicative of well-dispersed particles with a narrow (hydrodynamic) size distribution. For the amorphous sample, the particles were not as discrete and well-defined, as also evident from their structure from TEM (Fig 1), but they could also be readily dispersed in aqueous solvent and provided better hydrodynamic characteristics than their crystalline counterparts under the same conditions (Table 1). However, under ethanolic (parent/storage solvent) conditions, also the crystalline MnO exhibited narrow hydrodynamic size distributions (Table 1), indicative of discrete particulates. Whereas the amorphous MnOx net surface charge, as measured by the ζ-potential in HEPES buffer at pH 7.2 yielded a negative surface charge, -25.7±1.47 mV, due to the carboxylic acid groups resulting from the PAA used as capping agent, the crystalline sample exhibited a net neutral charge at neutral pH (Fig 2c), the characteristic isoelectic point of $Mn(OH)_2$ [27]; further corroborated by considering PVP does not contain chargeable groups. The net neutral charge at neutral pH is also reflected in the "worse" hydrodynamic size results in ddH_2O of these samples, due to the absence of strong repulsive forces as in the case of the negatively charged MnOx. The overall characteristics of the PVP and PAA capped suspensions have been summarized

in Table 1.

Table 1. Hydrodynamic characteristics (number mean, *n*=3) based on the intensity peak distribution for manganese oxide suspensions (aqueous and ethanolic) obtained with the use of capping agents.

Sample (Reaction conditions)	Hydrodynamic diameter in EtOH	Hydrodynamic diameter in H_2O
PVP 10min@240ºC	129±9 nm	383±84 nm
PVP 20min@240ºC	204±8 nm	349±42 nm
PVP 30min@240ºC	156±22 nm	411±191 nm
PAA 10min@240ºC	N/A	105±11 nm
PAA 20min@240ºC	N/A	178±42 nm
PAA 30min@240ºC	N/A	113±11 nm

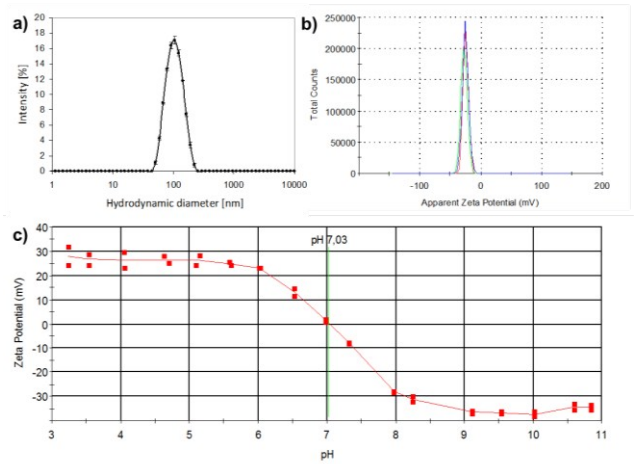

Fig. 2 Characterization of manganese oxide suspensions. **a)** Dynamic light scattering (intensity plot) of crystalline MnO prepared without capping polymers (30min@240◦C) in ddH_2O; **b)** zeta-potential of an amorphous MnOx (20min@240◦C) in HEPES buffer (25 mM, pH 7.2); **c)** isoelectric titration graph of sample *a)* yielding a net netural charge at physiological pH.

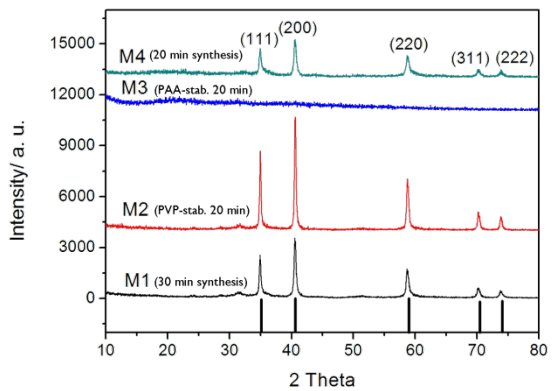

Fig. 3 XRD patterns for selected manganese oxide samples.

Based on dynamic light scattering data (Table 1), 20 min was concluded to be sufficient for obtaining of manganese oxide particles when stabilized by polymeric agents PVP or PAA. For confirmation of the crystalline phase (or absence thereof), selected samples were analyzed by XRD (Figure 3).

The diffraction patterns for samples produced via microwave digestion for 20 or 30 min at 240ºC without any additional polymer, showed clearly resolved peaks that could be indexed to a crystalline MnO phase [28]. The same pattern was observed for the PVP-stabilized sample digested for 20 min at 240ºC, whereas for the corresponding sample prepared with capping agent PAA, no distinctive XRD pattern could be found, indicative of an amorphous phase and in accordance with what was deduced from TEM characterization.

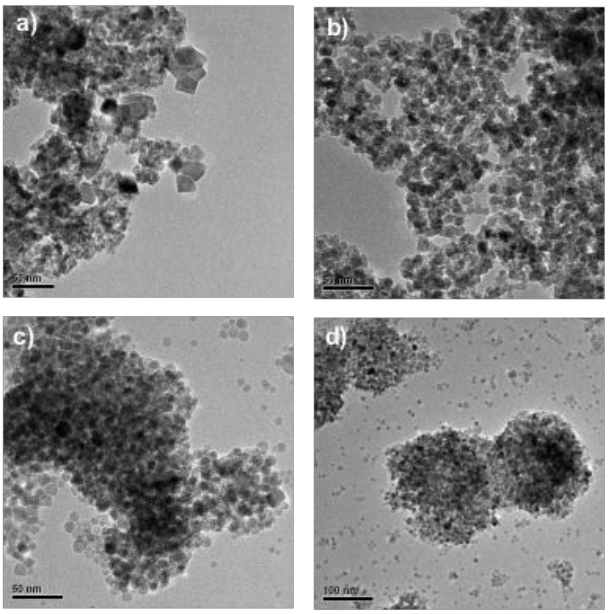

Fig. 4 Morphology investigation through TEM revealed more spherical-like particles for PVP-stabilized samples. MnO crystals formed without addition of polymers: a) 20 min reaction time & b) 30 min reaction time; MnO crystals formed with addition of PVP: c) 20 min reaction time & d) 30 min reaction time.

TEM analysis of the above samples (Figure 4) revealed some differences in size and morphology, also suggesting that 30 min provides for more uniform morphology than 20 min, whereas the addition of PVP seems to facilitate some additional morphology/size control inducing more uniform and spherical shape rather than crystal-like partculates; whereby 20 min microwave digestion is sufficient for the formation of ~10 nm MnO nanoparticles.

As can be deduced from these TEM images, especially when PVP is used as capping agent, there seems to coexist nanoclusters together with independent nanoparticles, which may explain why the individual particle diameter is about 10 nm but the hydrodynamic size (by DLS) is exceeding 200 nm (Table 1). In this case, the PVP thus seems to function primarily as a morphology inducer and/or growth regulator rather than an effective dispersion agent. Clearly, separate and almost spherical nanoparticles with diameters less than 10 nm have formed (Figures 4c&d), but to keep them properly separated also in the final suspension, either the PVP concentration would need to be optimized, or a second dispersion agent would need to be added,

or possibly some other suspension media could be used. It should be noted, however, that particle aggregation would also readily take place upon drying on the grids used for electron microscopy, due to the large surface energy of such small particles. Upon application in biological systems, further organic coating of the nanoparticles would also commonly come in question [3].

Relaxometric properties

To assess the suitability of the produced manganese oxides for MR imaging, the relaxometric properties of the as-prepared materials, in terms of their relaxation times *T*1 and *T*2 as a function of Mn concentration, was first determined using a minispec NMR spectrometer (Figure 5). *T*1 and *T*2 describe the longitudinal and transverse relaxation of excited protons, respectively; and a shorter relaxation time is associated with brighter (*T*1) or darker (*T*2) image intensity.

Remarkably, the relaxation times of the amorphous samples (Fig 5a&b) were significantly shorter than those of the crystalline particles down to extremely low values (*T*1 below 20 ms and *T*2 below 10 ms at high concentrations of Mn). The corresponding relaxivity plots (Fig 6a-c) revealed $r_{1,2}$ values of r_1= 15.6, 26.7, 24.9 mM^{-1} s^{-1} and r_2 = 30.8, 52.2, 39.1 mM^{-1} s^{-1} for the amorphous MnOx. The corresponding relaxivity values for the crystalline MnO (Supplementary Figure 1a,b) are r_1= 0.3, 0.09 mM^{-1} s^{-1} and r_2 = 6.7, 1.4 mM^{-1} s^{-1}, i.e. approximately an order of magnitude lower. These striking differences in relaxometric properties can be due to many reasons, related to different materials characteristics such as saturation magnetization, particle size and surface coating as well as dispersability in aqueous solvent [29-33]. For instance, when superparamagnetic particles are very small, their 1/*T*2 has shown to be proportional to particle size; whereas when the particles are large, 1/*T*2 will be proportional to the inverse particle size [29]. The slight deviations from linearity observed for most of the samples may well also be related to aggregation in solution, which, in turn, may very likely also partly be a consequence of time waiting dependence [32,33]. Time dependence in *T*2 relaxation time has been investigated for iron oxides, and found to be due to large particles generally having high saturation magnetization value and poor stability in water, which, in combination, may lead to aggregation under the 1.4T magnetic field used for relaxivity measurements of suspensions; whereby the relaxation time changes with time [32]. We have also recently shown the importance of an optimized surface functionalization for preventing aggregation of magnetic particles under a magnetic field [34]. These notions point to that careful surface engineering could be facilitative also from a relaxometric point of view.

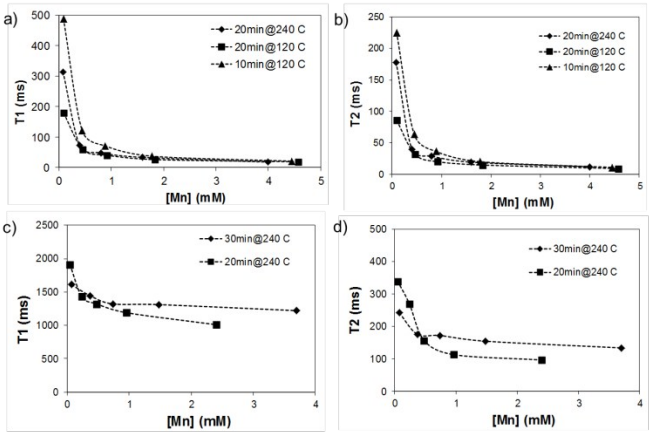

Fig. 5 Relaxivity measurements of as-prepared manganese oxides in water. a) & b) amorphous and c) & d) crystalline MnO. Measurements were performed on a minispec table-top NMR instrument.

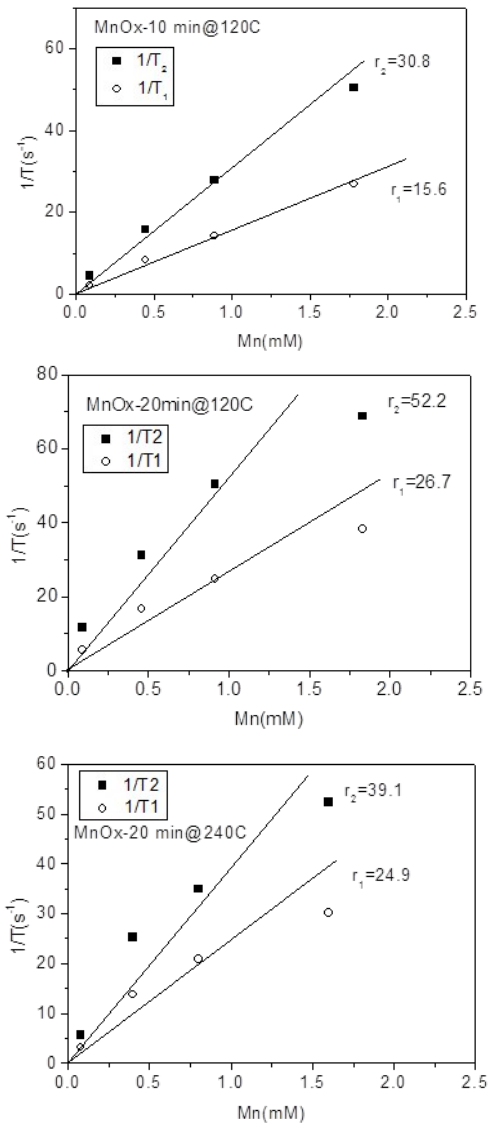

Fig. 6 Relaxivity plots for as-prepared amorphous MnOx prepared at different reaction times and tempereatures.

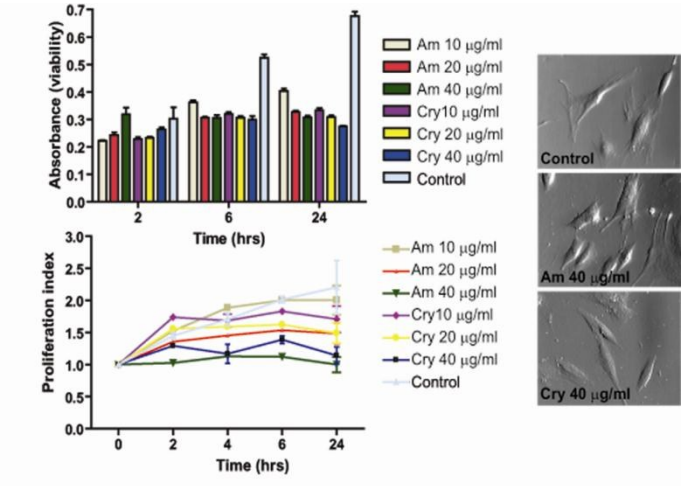

Fig. 7 Viability and proliferation of hMSC labeled with Mn-oxide particles.

Cytocompatibility

To ensure the feasibility of the produced particles for cellular labeling also in terms of cytocompatibility, we tested the effect on cell viability by labeling hMSCs for 2h with 10, 20, and 40 µg/ml of amorphous (PAA, 20 min@240◦C) or crystalline (no additives, 30 min@240◦C) particle samples. Viability/ proliferation was measured up to 24h after labeling. After 2h, there were no significant changes in viability, however a reduction of 20 % versus 50 % (non-treated cells) in viability was observed at 6h and 24 h after labeling respectively (Figure 6). As there was no significant decrease in viability over time within the individual treatments, this indicated that cells did not die but instead proliferation was halted. When the results were plotted as proliferation index, it became evident that proliferation was affected in a dose dependent manner. The cells treated with 40 µg/ml ceased to proliferate, while the cells labeled with 10 µg/ml continued to proliferate albeit slightly slower than non-treated cells. Amorphous particles demonstrated higher cytocompatibility than crystalline particles, and cells treated with 10 µg/ml amorphous particles continued to proliferate.

MR Imaging

MR imaging measurements showed similar results to the NMR spectrometer, where the amorphous particles displayed slightly higher relaxivity, indicated by shorter relaxation times at low concentrations (Figure 7). However, when examining the relaxometric properties of amorphous vs crystalline MnO(x) in agar, measured on the clinical 3 T MRI scanner, the difference between the amorphous and crystalline samples are not that remarkable as when measured as aqueous suspensions (Fig 5). The corresponding relaxivity values for agar-immobilized MnO(x) particles measured at 3 T were r_1 = 30.4 mM^{-1} s^{-1}, r_2 = 65.7 mM^{-1} s^{-1} for the amorphous MnOx, and r_1 = 10.0 mM^{-1} s^{-1}, r_2 = 65.0 mM^{-1} s^{-1} for the crystalline MnO. This indicates the differences in relaxivity observed in the aqueous suspension measurements may be chiefly related to colloidal stability in water; whereby aggregation of particles will lead to a decrease relaxivity. Indeed, the crystalline samples exhibited poorer dispersability properties (Table 1) as a result of the net neutral charge under these conditions (Fig 2c) as compared to the

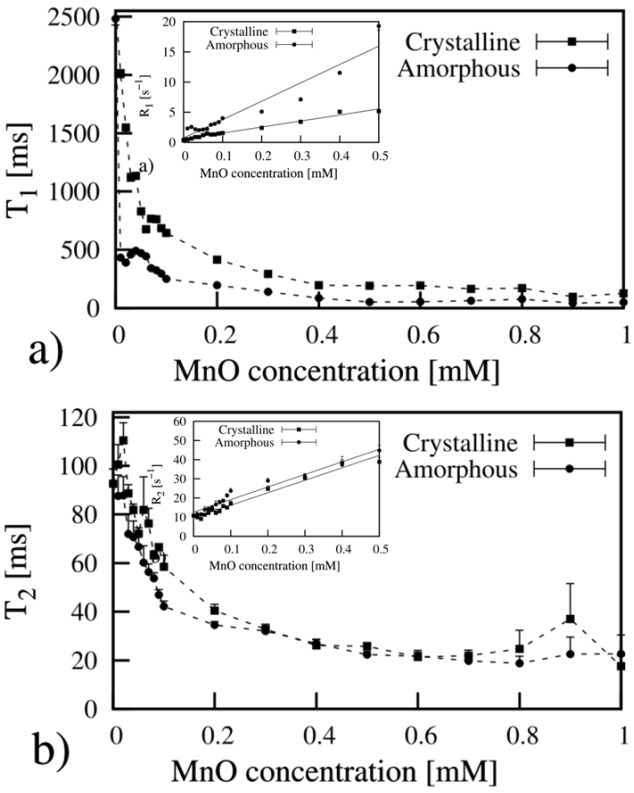

Fig. 8 Relaxation time measurements on manganese oxide particles in agar measured with a 3T MR-scanner. Insets show the corresponding relaxivity plots, resulting in relaxivity values of a) r_1 = 30.4 mM^{-1} s^{-1} (amorphous) and r_1 = 10.0 mM^{-1} s^{-1} (crystalline); b) r_2 = 65.7 mM^{-1} s^{-1} and r_2 = 65.0 mM^{-1} s^{-1}.

amorphous MnOx, which were electrostatically stabilized in water (Fig 2b). The corresponding MR image (Figure 9) of amorphous MnOx particles in agar demonstrates apparent differences in signal intensity profile relating to particle concentration (Figure 8). The relaxation times for labeled hMSCs are shown in Table 2. It is interesting to note that the reduction in *T*2 seemed more proficient than *T*1, even though MnO has to date mainly been put forward as a *T*1 contrast agent [23,24].

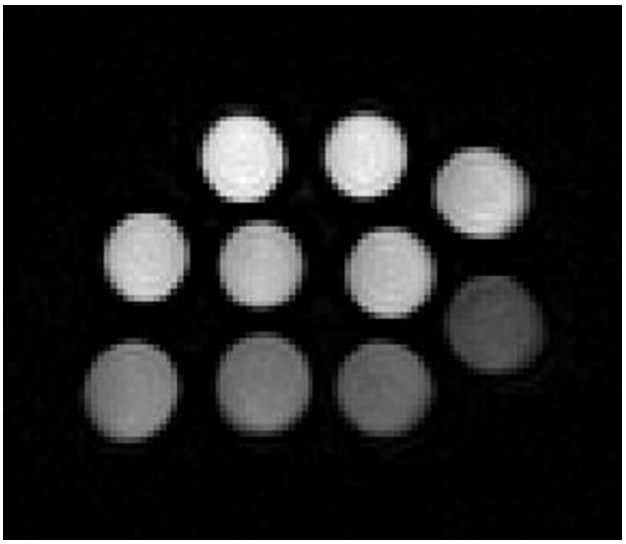

Fig. 9 3T MR image illustrating relaxation measurements. Slice was set to form a circular cross—section of the test tubes. Each test tube contains certain concentration of amorphous MnOx (bottom left corner: 0mM, increasing from left to right and from bottom to top with an interval of 0.01mM up to 0.1 mM) in agar.

Table 2. Relaxation times (*T*1, *T*2) for labelled hMSCs as measured on a 3T MRI scanner.

Labeled cell samples at 3T				
	T2 [ms]		T1 [ms]	
	mean	SD	mean	SD
Am 20 µg/ml	35,06	2,08	2040	55,08
Am 40 µg/ml	37,07	3,51	1986	46,03
Cry 20 µg/ml	34,51	1,49	1598	53,41
Cry 40 µg/ml	31,83	1,32	1257	42,96

Discussion

To overcome the known drawbacks of excessive signal loss with ferrous agents, other nanoparticles and small-molecular compounds such as manganese and gadopentate dimeglumine are under research. The current study was based on the production of novel manganese oxide nanostructures for cell labeling. In general, the purpose of all cellular MR imaging techniques is to visualize the cell without interpretational challenges with subcellular structures or molecules. Recently, in the published literature, a few applications have pointed out the ability of MR imaging to detect MnO [23-26, 35]. However, heterogenous sets of MnO solely or with adjunctive coating techniques were used, and therefore the results may not be comparable. Here, the feasibility of using amorphous and crystalline MnO as cellular labels for MR imaging was demonstrated on a 3T MRI scanner. Noteworthily, especially the amorphous MnOx exhibited promising relaxometric properties; and to the best of our knowledge, amorphous MnOx, which is traditionally used in catalysis and manganese oxide electrodes, has not been previously reported to be used in related applications. Due to the extraordinary relaxometric properties determined, a novel notion depicted on MR images both using agar and *in vitro* hMSCs, further studies using amorphous MnOx for cell labeling are justified.

The polyol process has cleared ground amongst inorganic nanoparticle syntheses especially when biomedical applications are aimed for, due to the inherently hydrophilic particles that are produced as a result of the hydroxyl (-OH) groups that are formed on the surface by a layer of polyol molecules [7]. The polarity of the polyols moreover offer the ability to dissolve various inorganic salts, acts as the reducing agent for many kinds of metal ions for the synthesis of metal and metal oxide nanoparticles, and furthermore, the high boiling point enables elevated temperature conditions which, in turn, may improve the reactivity of the used reactants [17]. Synergistically, carrying out the synthesis with the aid of microwave irradiation offers a striking reduction of reaction times as opposed to conventional heating (oil bath or autoclave) from hours or days to minutes, allowing for a time- and energy-saving process [14]. Superior colloidal stability in aqueous environment could potentially still be achieved by addition of a polyelectrolyte such as PAA, the chains of which can strongly coordinate to metal ions such as iron on a nanocrystal surface, while uncoordinated carboxylic acid groups can extend into the surrounding water [10]. In the present case, a change in pH was exerted by the polyacid, inducing the formation of an amorphous phase over a crystalline one. Shifting PAA to the strong coordinating agent PVP, an amphiphilic, nonionic polymer, widely used to improve the colloidal stability of various particle types as it is known to adsorb well onto a broad range of different materials [36], produced crystalline materials as expected. Here, the PVP seemed to rather function as a morphology (shape) inducer and size regulator, leading to spherical nanocrystals of less than 10 nm in diameter. Further optimization of surface coating procedures will facilitate the application of the produced Mn-based nanostructures as cellular labels from a colloidal stability, cytocomptability and thus, ultimately, also relaxivity point of view.

Conclusions

In conclusion, novel, “green” and fast-processed manganese oxide nanostructures, both amorphous and crystalline, were developed using a combination of the “polyol” synthetic approach with microwave digestion. In both cases, a stable suspension of particles of nanometric dimensions was successfully produced. The amorphous material in particular exhibited prominent relaxometric properties, although both crystalline (MnO) and amorphous (MnOx) materials provided sufficient contrast enhancement on MR images; and thus we envision either of the techniques to be feasible and well suited for producing Mn-based nanostructures for cell labeling.

Acknowledgements

The Instrument Centre of Shanghai Jiao Tong University, P.R. China, is acknowledged for instrument use. MSc Natalie Råtts is acknowledged for assistance in the cell biological work. Svenska Tekniska Vetenskapsakademien i Finland r.f., Tekniikan Edistämissäätiö, and the Academy of Finland (project #260599) are acknowledged for financial support (J.M.R.)

Notes and references

[a] *Pharmaceutical Sciences Laboratory, Faculty of Science and Engineering, Åbo Akademi University, Turku, Finland.. Tel: +358-2-215 3255; E-mail: jerosenh@abo.fi*
[b] *Department of Diagnostic Radiology, Oulu University Hospital, Oulu, Finland.*
[c] *Department of Radiology, Helsinki University Hospital, Helsinki, Finland.*
[d] *Department of Anatomy and Clinical Research Center, University of Oulu, Oulu, Finland.*
[e] *University of Oulu, Department of Anatomy and Cell Biology and Oulu University Hospital, Medical Research Center and Respiratory Research Unit, Finland.*
[f] *Cell Biology, Faculty of Science and Engineering, Åbo Akademi University, Turku, Finland.*
[g] *Turku Centre for Biotechnology, University of Turku and Åbo Akademi University, Turku, Finland.*
[h] *Nano Biomedical Research Center, Med-X Research Institute and School for Biomedical Engineering, Shanghai Jiao Tong University, Shanghai, P.R. China.*
[i] *Chongqing University, College of Bioengineering, Chongqing, China.*
[j] *Laboratory for Physical Chemistry, Faculty of Science and Engineering, Åbo Akademi University, Turku, Finland..*
[k] *Department of Biomedical Engineering, Technical University of Eindhoven, The Netherlands. E-mail: C.M.Sahlgren@tue.nl*
[l] *Department of Radiology,Turku University Hospital, Turku, Finland. Tel: +358-2 313 1975; E-mail: roberto.blanco@oulu.fi*
[§] *equal contribution.*

† Electronic Supplementary Information (ESI) available. See DOI: 10.1039/b000000x/

1 L. Ferreira, J.M. Karp, L. Nobre and R. Langer, *Cell Stem Cell*, 2008, **3**, 136.
2 C. Sun, J.S.H. Lee and M. Zhang M, *Adv. Drug Delivery Rev*, 2008, **60**, 1252.
3 A. Taylor, K.M. Wilson, P. Murray, D.G. Fernig and R. Lévy, *Chem Soc Rev*, 2012, **41**, 2707.
4 R. Weissleder, G. Elizondo, J. Wittenberg, C.A. Rabito, H.H. Bengele and L. Josephson, *Radiology*, 1990, **175**, 489.
5 J.W. Bulte and D.L. Kraitchman, *NMR Biomed*, 2004, **17,** 484.
6 Z. Li, Q. Sun and M. Gao, *Angew Chem Int Ed*, 2005, **44**, 123.
7 J. Wan, W. Cai, X. Meng and E. Liu, *Chem Commun*, 2007, 5004.
8 W. Xiao, H.-C. Gu, D. Li, D. Chen, X. Deng, Z. Jiao and J. Lin, *J Magnetism Magnetic Mater*, 2012, **324,** 488.
9 E. Wetterskog, M. Agthe, A. Mayence, J. Grins, D. Wang, S. Rana, A. Ahniyaz, G. Salazar-Alvarez and L. Bergström, *Sci. Technol. Adv. Mater*, 2014, **15**, 055010.
10 J. Ge, Y. Hu, M. Biasini, C. Dong, J. Guo, W.P. Beyermann and Y. Yin, *Chem Eur J*, 2007, **13,** 7153.
11 C. Cheng, Y. Wen, X. Xu and H.-C. Gu, *J Mater Chem*, 2009, **19**, 8782.
12 Y. Sun, Y. Yin, B.T. Mayers, T. Herricks and Y. Xia, *Chem Mater*, 2002, **14,** 4736.
13 S.H. Im, Y.T. Lee, B. Wiley and Y. Xia, *Angew Chem Int Ed*, 2005, **44,** 2154.
14 I. Bilecka, I. Djerdj and M. Niederberger, *Chem Commun*, 2008, 886.
15 S.E. Skrabalak, B.J. Wiley, M. Kim, E.V. Formo and Y. Xia, *Nano Lett*, 2008, **8,** 2077.
16 X. Jia, D. Chen, X. Jiao and S. Zha, *Chem Commun*, 2009, 968.
17 C. Cheng, F. Xu and H.-C. Gu, *New J Chem*, 2011, **35**, 1072.
18 I. Bilecka and M. Niederberger, *Nanoscale*, 2010, **2,** 1358.
19 W. Guan, W. Gu, L. Ye, C. Guo, S. Su, P. Xu, M. Xue, *Int J Nanomed*, 2014, **9,** 5071.
20 J.W. Bulte, *AJR Am J Roentgenol*, 2009, **193**, 314.
21 H.S. Thomsen, *Eur Radiol*, 2006, **16**, 2619.
22 J. Perez-Rodriguez, S. Lai, B.D. Ehst, D.M. Fine and D.A. Bluemke, *Radiology*, 2009, **250,** 371.
23 H. Na, J. Lee, K. An, Y. Park, M. Park, I.S. Lee, D.-H. Nam, S.T. Kim, S.-H. Kim, S.-W. Kim, K.-H. Lim, K.-S. Kim, S.-O. Kim and T. Hyeon, *Angew Chem Int Ed*, 2007, **46**, 5397.
24 A. Gilad, P. Walczak, M. McMahon, H. Na, J. Lee, K. An, T. Hyeon, P. van Zijl and J. Bulte, *Magnetic Resonance in Medicine*, 2008, **60,** 1.
25 K.H. Bae, K. Lee, C. Kim and T.G. Park, *Biomaterials*, 2011, **32,** 176.
26 T. Kim, E. Momin, J. Choi, K. Yuan, H. Zaidi, J. Kim, M. Park, N. Lee, M.T. McMahon, A. Quinones-Hinojosa, J.W.M. Bulte, T. Hyeon and A.A. Gilad, *J Am Chem Soc*, 2011, **113,** 2955.
27 G.A. Parks, *Chem Rev*, 1965, **65**, 177.
28 F. Gao, J.-Y. Qu, Z.-B. Zhao, Y.-F. Dong, J. Yang, Q, Dong, J.-S. Qiu, *New Carbon Materials*, 2014, **29**, 316.
29 D.-X. Chen, N. Sun, H.-C. Gu, *Journal of Applied Physics*, 2009, 063906.
30 L.E.W. LaConte, N. Nitin, O. Zurkiya, D. Caruntu, C.J. O'Connor, X. Hu, G. Bao, *Journal of Magnetic Resonance Imaging*, 2007, **26**, 1634.
31 H. Duan, M. Kuang, X. Wang, Y.A. Wang, H. Mao, S. Nie, *Journal of Physical Chemistry C*, 2008, **112**, 8127.
32 N. Sun, D.-X.Chen, H.-C.Gu, X.-L.Wang, Journal of Magnetism and Magnetic Materials, 2009, **321,** 2971.
33 D.-X. Chen, N.Sun, Z.-J.Huang, C.-M.Cheng, H.Xub, H.-C.Gu, *Journal of Magnetism and Magnetic Materials*, 2010, **322,** 548.
34 T Gulin-Sarfraz, J. Zhang, D. Desai, J. Teuho, J. Sarfraz, H. Jiang, C. Zhang, C. Sahlgren, M. Lindén, H. Gu, J.M. Rosenholm, *Biomaterials Science*, 2014, **2**, 1750.
35 C. Liang, C. Wang, Z. Liu, *Particle & Particle Systems Characterization*, 2013, **30**, 1006.
36 C. Graf, D.L.J. Vossen, A. Imhof and A. van Blaaderen, *Langmuir*, 2003, **19**, 6693.